Evaluation of 3D gradient filters for estimation of the surface orientation in CTC

Tarik A. Chowdhury, Ovidiu Ghita and Paul F. Whelan
Vision Systems Group
School of Electronic Engineering
Dublin City University
Dublin 9, Ireland
tarik@eeng.dcu.ie

Abstract

The extraction of the gradient information from 3D surfaces plays an important role for many applications including 3D graphics and medical imaging. The extraction of the 3D gradient information is performed by filtering the input data with high pass filters that are typically implemented using 3×3×3 masks. Since these filters extract the gradient information in small neighborhood, the estimated gradient information will be very sensitive to image noise. The development of a 3D gradient operator that is robust to image noise is particularly important since the medical datasets are characterized by a relatively low signal to noise ratio. The aim of this paper is to detail the implementation of an optimized 3D gradient operator that is applied to sample the local curvature of the colon wall in CT data and its influence on the overall performance of our CAD-CTC method. The developed 3D gradient operator has been applied to extract the local curvature of the colon wall in a large number CT datasets captured with different radiation doses and the experimental results are presented and discussed.

Keywords: 3D gradient operators, CTC, polyp detection, local curvature.

1 Introduction

Computer Tomography Colonagraphy (CTC) [1-4] is a rapidly evolving minimally invasive technique for early detection of colorectal polyps and nowadays the medical community views this medical procedure as a viable alternative to optical colonoscopy. As the performance of the CT imaging modalities is constantly improving, recent studies have demonstrated that the sensitivity in polyp detection offered by the CTC compares favorably with the sensitivity offered by the optical colonoscopy [5,6]. With the introduction of the new generation of multi-slice CT scanners that are able to produce high resolution CT data, the CT datasets generate a sheer volume of information required to be interpreted by the radiologist and this task is performed by analyzing either the 2D axial views or the 3D surface of the colon wall. The visual analysis of the CT data is a time consuming procedure and the examination results are biased by the subjectivity and the experience of the radiologists. This fact encouraged the development of automated computer aided detection (CAD)-CTC systems that are able to produce reproducible results with high sensitivity in detection of clinically significant polyps (>5mm). The main problem associated with the current range of developed CAD-CTC systems is the large number of false positives that are generated by other colon structures that mimic the shapes of the polyps (haustral folds, residual material, etc) [7-9]. The large number of false positives is generated by the subtle difference in shape between the polyps and other colon structures but also by the errors in the assessment of the local curvature (convexity) of the colon wall. In this paper we attempt to evaluate the contribution of the image noise (and the partial volume effects generated by the relatively low resolution in the z axis) in the estimation of the local curvature of the colon wall.

In order to determine the surface orientation we need to extract first the local derivatives from the 3D data. In 2D data the normal vector to a curve can be calculated by computing the local derivatives in the x and y direction using high pass local operators. The CTC datasets are 3D and

most algorithms that perform automatic identification of colorectal polyps evaluate the local curvature of the colon wall by calculating in 3D the partial derivatives [7]. As the polyps are structures with a well-defined convex appearance we need to evaluate the measure of convexity by evaluating the normal intersection around suspicious colon structures. Nonetheless, this method will be successful if we are able to accurately extract the surface orientation, i.e. the normal vector. In this regard an elegant solution to this problem is the extension of the calculation of the normal vector in 2D to 3D data. In this regard, Zucker and Hummel [10] proposed a mathematical model to determine the optimal 3D gradient operators. In their formulation they determined the masks of the gradient operator using a functional analysis and their theory was just in fact the generalization of the ubiquitous 2D Sobel operator [11]. The optimal gradient operator described in their paper is a 3×3×3 anti-symmetric operator that is applied in 3 different directions (the Zucker-Hummel operator uses radial functions that smooth the calculated gradient. This will have a positive effect in cases where the Zucker-Hummel operator is applied to noisy data). One limitation of this operator is the small kernel that is used to sample the gradient in x, y, z directions and as a consequence the results are only modest in extracting the local orientation for complex surfaces such as roofs or cavities. This is highlighted in our experiments where is indicated that the Zucker-Hummel operator is in many cases outperformed by the standard 3D Sobel operator. The aim of this paper is to evaluate the influence of the selection of the gradient operator on the overall performance of our CAD-CTC and to detail the mathematical model that will allow us to implement optimized 3D gradient operators.

2 Mathematical background of gradient detection

In image processing the gradient operators are widely used to identify strong features in the image such as edges or the local orientation of the curves and surfaces. The extraction of local derivative from a continuous signal can be done by applying directly the well-known derivative formula:

$$Der(f(x)) = \lim_{\alpha \to 0} \frac{f(x+\alpha) - f(x)}{\alpha} \tag{1}$$

When designing a gradient operator we should bear in mind that the image data is discrete and we cannot apply the finite differences without compromising the accuracy of the gradient approximation [12-15]. Thus we have to assume that the original continuous optical signal that generates the image has been uniformly sampled at a rate of T samples per length. Using the Nyquist sampling theorem the continuous signal can be reconstructed from these discrete samples as follows:

$$f(x) = \sum_{k=1}^{N} f[k]s(x - KT), \; s(x) = \frac{\sin x}{x} \tag{2}$$

In equation 2 the term $f[k]$ represent the discrete sampled signal and $s(x)$ defines the sampling function that can be approximated with the *sinc* function. Hence, to obtain the gradient of the discrete signal we have to derivate the reconstructed signal $f(x)$ that is depicted in equation 2.

$$Der(f(x)) = \sum_{k=1}^{N} f[k]der(s(x - KT)) = \sum_{k=1}^{N} f[k]s'(x - KT) \tag{3}$$

where s' represents the derivative of the *sinc* function. As the derivative of the *sinc* function is dependent on the sampling frequency, it is worth noting that the spectrum of the discrete signal is bounded by $2\pi / T$ that is in agreement with the sampling theorem. We note that the derivative of *sinc* signal decays relatively slowly and the implementation of an optimal gradient filter would require large filters that are not feasible to be applied in practice due to the onerous computational cost required to extract the partial derivatives. Next, we will introduce a practical method to design one-dimensional (1-D) gradient filters whereas the generalization to multiple dimensions is a

relatively simple task. In order to design gradient operators that are to be applied to discrete signals we have to consider several constraints. The vision literature indicates that the gradient filters are anti-symmetric and usually have an odd order. Thus, the 1-D gradient filter can be represented in the following generic form:

$$d(k) = [d_{-N}, d_{-N+1}, ..., d_{-1}, 0, d_1, ..., d_{N-1}, d_N], \quad d_{-k} = -d_k, \quad k = 1, ..., N \tag{4}$$

In order to design 1-D derivative filters we need to impose several constraints for parameters d_k as illustrated in the following expressions [14]:

$$\sum_{k=-N}^{N} d_k = 0 \tag{5}$$

$$\sum_{k=-N}^{N} d_k k = 0 \tag{6}$$

In this way, equation 5 translates in the requirement that the derivative filter should have the sum of the coefficients equal to 0, while equation 6 can be used to select the values for d_k coefficients. The derivative operator has to fulfill the condition illustrated in equation 5 to achieve insensitivity to DC signals. Since the derivative filters are anti-symmetric the first coefficient of the operator can be determined using the following relationship:

$$d_1 = \frac{1}{2} - \sum_{k=2}^{N} d_k \tag{7}$$

Using the formulas illustrated in equations 4 to 7, the 5×5×5 derivative filter that is applied to extract the gradient in the x direction has the following mask [-1 8 0 -8 1]/12 • [1 4 6 4 1]/16, where • defines the convolution operator. To extract the gradient for other directions we need to rotate the 5×5×5 mask in the direction required for a particular axis. It can be noted that this operator, as expected, represents the direct extension of the 5×5 Sobel operator to the 3D case. Using equations 5 to 7, we have developed a new 5×5 gradient operator that implements a two-peak operator. Since the gradient operator has two lobes it will provide improved performance when applied to data with step discontinuities or 3D CT datasets defined by a low signal to noise ratio such as the low-dose CT data.

−.125	−.25	−.5	−.25	−.125		−.25	−.5	−1.0	−.5	−.25
−.25	−.5	−1.0	−.5	−.25		−.5	−1.0	−2.0	−1.0	−.5
−.5	−1.0	−2.0	−1.0	−.5		−1.0	−2.0	−4.0	−2.0	−1.0
−.25	−.5	−1.0	−.5	−.25		−.5	−1.0	−2.0	−1.0	−.5
−.125	−.25	−.5	−.25	−.125		−.25	−.5	−1.0	−.5	−.25

$0_{5\times5}$

.25	.5	1.0	.5	.25	.125	.25	.5	.25	.125
.5	1.0	2.0	1.0	.5	.25	.5	1.0	.5	.25
1.0	2.0	4.0	2.0	1.0	.5	1.0	2.0	1.0	.5
.5	1.0	2.0	1.0	.5	.25	.5	1.0	.5	.25
.25	.5	1.0	.5	.25	.125	.25	.5	.25	.125

Figure 1. The masks of the 5×5×5 3D OptDer operator to extract the gradient in the z axis (the mask 0_{5x5} indicates a 5×5 mask where all elements are zero).

In our experiments we have evaluated the efficiency of several filters including the 3×3×3 Zucker-Hummel operator, 5×5×5 Sobel operator and 5×5×5 optimized operator – OptDer filter (is a two peak derivative operator. For more details about the implementation of optimal derivative filters refer to [12,13]). A particular interest we had in assessing the performance of these gradient operators when applied to CTC datasets that have been acquired with different x-ray dose levels

(the lower the radiation dose the higher the image noise). However in our experiments it has became clear that the 3×3×3 gradient masks are inefficient in sampling the correct curvature of the colon wall when dealing with irregular surfaces. The experimental data indicated that the optimized 5×5×5 gradient operator was able to return improved performance (this operator has been designed using the masks illustrated in Figure 1). The measurements were performed on CTC prone and supine views where the reconstruction interval was set to 1.5mm. The tests were conducted on phantom (synthetic) data and on real patient data. Of particular interest was the evaluation of the level of false positives detected by the automated CAD-CTC system and a detailed performance of our system is illustrated in Tables 1 to 5 where different gradient operators are evaluated.

3 CAD-CTC Polyp Detection Algorithm

We have developed an automated CAD-CTC method designed to identify the colorectal polyps in CT data [16] that evaluates the local morphology of the colon wall. Initially, the colon is segmented using a seeded 3D region growing algorithm that was applied to identify the interface between the air voxels and the colon tissue, which assures the extraction of the colon wall. After the identification of the colon wall, for each colon wall voxel the surface normal vector is calculated using the Hummel-Zucker operator, Sobel and OptDer operator. The normal vectors sample the local orientation of the colon surface and the suspicious candidate structures that may resemble polyps are extracted using a convexity analysis where the colon suspicious surfaces are detected by evaluating the distribution of the normal vectors intersections in the 3D space (for a detailed description of this algorithm refer to [16]). This method is able to correctly identify all polyps above 3mm but it is worth noting that this is achieved at the cost of a high level of false positives. In order to reduce the level of false positives, statistical features [16] including the standard deviation of surface variation, ellipsoid fitting error, sphere fitting error, three axes of the ellipsoid and the Gaussian sphere radius are calculated for each candidate surface that has been identified by the convexity method described before. These features are used as inputs for a nearest neighbor classifier that is trained to decide whether the surface under investigation belongs to a polyp or a fold. The classifier was trained using a collection of 64 polyps and 354 folds that were selected by a radiologist from Mater Misericordiae Hospital, Dublin.

4 Results and Discussions

In our tests we have used 52 standard dose (100mAs) patient datasets (prone and supine views) with 75 polyps, 9 low dose (13-50mAs) patient data with 2 small polyps and phantom data (low-dose and standard dose) with 48 polyps of various sizes and shapes. All patients were scanned at 120kVp, 13mAs-100mAs, 2.5mm collimation, 3mm slice thickness, 1.5mm reconstruction interval, and 0.5s gantry rotation. The CT acquisition was performed with the patient head-first supine position and then repeated with the patient in the prone position. The CT protocol mentioned before generates CT datasets where the number of axial slices is in the range 200-350 and is dependent on the height of the patient.

Table 1: Sensitivity for synthetic phantom data (polyps >=10mm).

mAs	Total	Sensitivity (%)		
		Zucker	Sobel	OptDer
100	14	100	100	100
40	14	100	100	100
30	14	100	92.85	100
20	14	100	100	100
13	14	92.85	92.85	100

Table 2: Sensitivity for synthetic phantom data (polyps [5-10)mm).

mAs	Total	Sensitivity (%)		
		Zucker	Sobel	OptDer
100	20	100	100	100
40	20	100	100	100
30	20	95	90	95
20	20	100	100	95
13	20	95	95	100

Table 3: Sensitivity for synthetic flat polyps.

mAs	Total	Sensitivity (%)			False Positive per dataset		
		Zucker	Sobel	OptDer	Zucker	Sobel	OptDer
100	9	55	55	44.44	1	1	1
40	9	33.33	33.33	44.44	2	1	1
30	9	44.44	44.44	55	0	2	2
20	9	11.11	33.33	44.44	2	2	2
13	9	22.22	22.22	44.44	2	2	3

Table 4: Sensitivity for polyps >=5mm in real patient standard dose (100mAs) data.

mAs	Total	Sensitivity (%)			False Positive per dataset		
		Zucker	Sobel	OptDer	Zucker	Sobel	OptDer
100	18	88.89	88.89	88.89	4.32	4.69	4.71

Table 5: Sensitivity for polyps <5mm in real patient's standard and low dose data

mAs	Total	Sensitivity (%)		
		Zucker	Sobel	OptDer
100	48	60.41	60.41	68.75
13-40	2	50	100	100

When the CAD-CTC system was applied on phantom data the OptDer operator shows 100% sensitivity for polyp >=10mm for datasets acquired with radiation doses in the range 100-13mAs where the Zucker-Hummel and Sobel operators shows 92.85% sensitivity at 30mAs and 13mAs radiation doses (see Table-1). Figure 2(a) illustrates the 3D surface extraction for a 12mm polyp when the Zucker-Hummel operator was applied for detection of the surface normal vectors and Figure 2(b) shows the surface extraction when the OptDer operator has been used. Figure 3 illustrate the surface extraction for an 8 mm phantom polyp from a dataset scanned with 13mAs. It can be noted that in both cases the CAD-CTC system achieved a more accurate surface extraction when the OptDer operator was employed. Due to incomplete surface segmentation our CAD-CTC system missed the polyp illustrated in Figure 2 when the Zucker-Hummel operator was used to extract the surface normal vectors (see Table 1), whereas the polyp was correctly detected when the OptDer operator was applied. In Figures 2 and 3 it can be also observed that the OptDer operator generates better surface normal concentration than the Zucker-Hummel operator. The application of the OptDer operator to extract the surface normal vectors offers better detection for polyps in the range 5-10mm than the Sobel operator (see Table 2). It also

provides a better detection of flat polyps when compared to the performance of the Zucker-Hummel and Sobel operators (see Table 3). When the Zuker-Hummel, Sobel and OptDer operators were used to calculate the surface normals of the colon wall for standard dose real patient datasets, the sensitivities for the detection of polyps >=5mm were 88.89% (see Table 4) for all operators, but the OptDer operator provides higher sensitivity (see Table 5) in the detection of small polyps (<5mm) than the other two operators. Table 5 indicates that the overall sensitivity for polyp detection was highest when the OptDer operator was used and the experimental data indicates that this operator outperformed the Zucker-Hummel and the Sobel operators especially when the system is applied to low-dose datasets. The level of noise sampled by the standard deviation calculated in a local 5×5×5 neighborhood increased with a factor of 2.67 (SD = 26.59 for 100mAs and SD = 70.95 for 13mAs) when the scan was performed at 13mAs when compared to the case when the phantom was scanned with 100mAs radiation dose. The relation between the noise level and the radiation dose is illustrated in Figure 4.

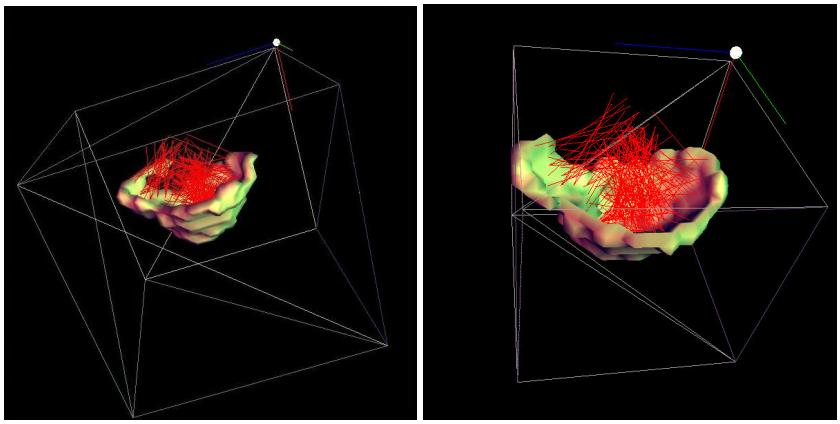

(a) (b)

Figure 2. 3D surface extraction of a 12mm phantom polyp (radiation dose 13mAs). (a) The 3D surface extracted by the CAD-CTC system using the Zucker-Hummel operator. (b) The 3D surface extracted by the CAD-CTC system using the OptDer operator.

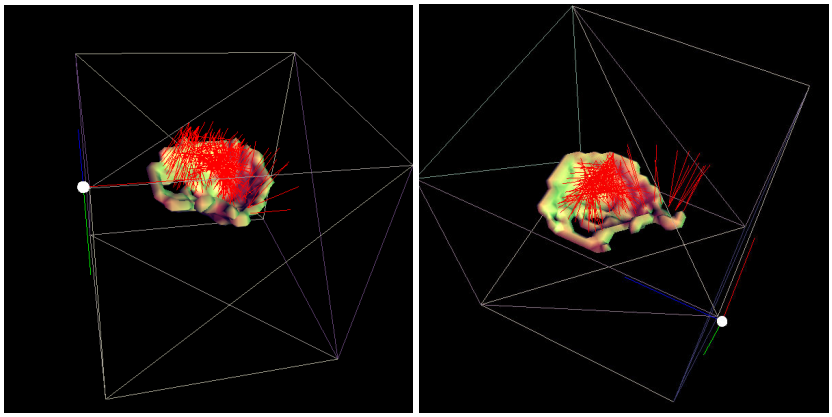

(a) (b)

Figure 3. 3D surface extraction of a 12mm phantom polyp (radiation dose 13mAs). (a) The 3D surface extracted by the CAD-CTC system using the Zucker-Hummel operator. (b) The 3D surface extracted by the CAD-CTC system using the OptDer operator.

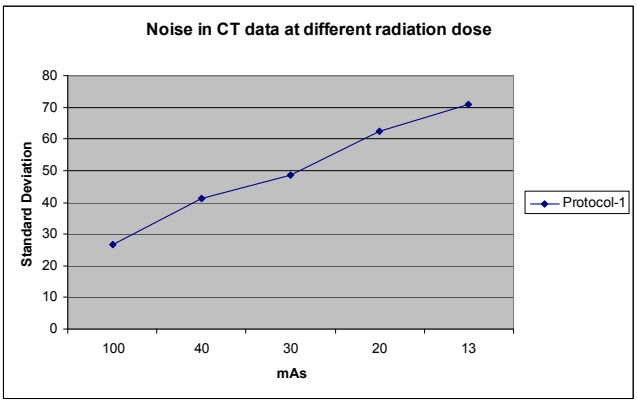

Figure 4. The relationship between the noise level and the radiation dose.

5 Conclusions

In this paper we have addressed the problem of robust calculation of the surface curvature in 3D CT data. As numerous automated CAD-CTC systems identify the colorectal polyps based on analysing the local convexity of the colon surface, one of the most important steps in this analysis is the precise identification of normal vector. In this regard, we have investigated a number of 3D gradient operators and we have conducted the experiments on a large number of synthetic and real patient data. Experimental data indicated that the commonly used 3D gradient operators such as Zucker-Hummel and Sobel fail to correctly determine the normal vector when dealing with datasets characterized by a low signal to noise ratio. To address this problem we have proposed a new gradient operator that was able to return better performance when applied to CT data that is acquired with different radiation dose levels.

Acknowledgements

We would like to acknowledge the contributions of our clinical partners in this project: Dr. Helen Fenlon (Department of Radiology) and Dr. Padraic MacMathuna (Gastrointestinal Unit) of the Mater Misericordiae Hospital, Dublin. This work was supported under an Investigator Programme Grant (02/IN1/1056) by Science Foundation Ireland (SFI).

References

[1] Vining D.J, Gelfand D.W., Bechtold R.E (1994), Technical feasibility of colon imaging with helical CT and virtual reality, AJR, 162, 104.

[2] Johnson C.D., Hara A.K., Reed J.E. (1998), Virtual endoscopy: what's in a name?, AJR, 171, 1201-2.

[3] Hara A.K., Johnson C.D., Reed J.E., Ahlquist D.A., Nelson H., Ehman R.L., McCollough C., Ilstrup D.M. (1996), Detection of Colorectal Polyps by CT Colonography: Feasibility of a novel technique, Gastroenterology, vol. 100:284-290.

[4] Johnson C.D., Hara A.K. (2000), CT colonography: the next colon screening examination?, Radiology, vol. 216, pp. 331-341.

[5] Fenlon H.M., Nunes D.P., Schroy P.C., Barish M.A., Clarke P.D., Ferrucci J.T. (1999), A comparision of virtual and convention colonoscopy for the detection of colorectal polyps, N. Engl J Med, 341:14961503.
[6] Pickhardt P.J., Choi J.R., Hwang I., Butler J.A., Puckett M.L., Hildebrandt H.A., Wong R., Nugent P.A., Mysliwiec P.A., Schindler W.R. (1997), Virtual colonoscopy for colorectal polyp detection, RBM; 19(5): 143-147.
[7] Summers R.M., Johnson C.D., Pusanik L.M., Malley J.D., Youssef A.M., Reed J.E. (2001). Automated polyp detection at CT colonography: Feasibility assessment in a human population, Radiology 219:51-59.
[8] Yoshida H., Masutani Y., MacEneaney P., Rubin D.T., Dachman A.H. (2002), Computerized detection of colonic polyps at CT colonography on the basis of volumetric features: Pilot study, Radiology, vol. 222, pp. 327-336.
[9] Paik D.S., Beaulieu C.F. et al. (2004), Surface normal overlap: a computer-aided detection algorithm with application to colonic polyps and lung nodules in helical CT, IEEE Transactions on Medical Imaging, 23(6):661-675.
[10] Zucker S.W., Hummel R.A. (1981), A Three-Dimensional edge operator, IEEE Transactions on Pattern Analysis and Machine Intelligence, 3(3), pp.324-331.
[11] Whelan P.F., Molloy D. (2000), Machine Vision Algorithms in Java: Techniques and Implementation, Springer (London), ISBN 1-85233-218-2
[12] Farid H., Simoncelli E.P. (2004), Differentiation of Multi-Dimensional Signals, IEEE Transactions on Image Processing, 13(4):496-508.
[13] Simoncelli E.P. (1994), Design of multi-dimensional derivative filters, IEEE International Conference on Image Processing, vol. 1:790-793.
[14] Jahne B., Scharr H., Korkel S. (1999), Principles of filter design, Handbook of Computer Vision and Applications, Academic Press.
[15] Freeman W.H., Adelson E. H (1991), The design and use of steerable filters, IEEE Transactions on Pattern Analysis and Machine Intelligence, 13:891-906.
[16] Chowdhury T.A., Ghita O., Whelan P.F. (2005), A statistical approach for robust polyp detection in CT colonography, 27th Annual International Conference of the IEEE Engineering in Medicine and Biology Society, 1-4 September 2005, Shanghai, China